Robotica (2022), **40**, pp. 2152–2167
doi:10.1017/S0263574721001582

CAMBRIDGE UNIVERSITY PRESS

RESEARCH ARTICLE

Conceptual design and error analysis of a cable-driven parallel robot

Jiaxuan Li[1], Yongjie Zhao[1,*], Qingqiong Tang[1], Wei Sun[1], Feifei Yuan[1] and Xinjian Lu[2]

[1]Department of Mechatronics Engineering, Shantou University, Shantou City, Guangdong 515063, P. R. China and
[2]Guangdong Goldenwork Robot Technology Ltd, Foshan City, Guangdong 528226, P. R. China
*Corresponding author. E-mail: meyjzhao@stu.edu.cn

Received: 8 June 2021; **Revised:** 19 September 2021; **Accepted:** 12 October 2021; **First published online:** 19 November 2021

Keywords: cable-driven parallel robot, conceptual design, kinematics, error analysis, sensitivity coefficient

Abstract

This paper develops the conceptual design and error analysis of a cable-driven parallel robot (CDPR). The earlier error analysis of CDPRs generally regarded the cable around the pulley as a center point and neglected the radius of the pulleys. In this paper, the conceptual design of a CDPR with pulleys on its base platform is performed, and an error mapping model considering the influence of radius of the pulleys for the CDPR is established through kinematics analysis and a full matrix complete differential method. Monte Carlo simulation is adopted to deal with the sensitivity analysis, which can directly describe the contribution of each error component to the total orientation error of the CDPR by virtue of the error modeling. The results show that the sensitivity coefficients of pulleys' geometric errors and geometric errors of the cables are relatively larger, which confirms that the cable length errors and pulleys' geometric errors should be given higher priority in design and processing.

1. Introduction

Cable-driven parallel robot (CDPR) is a kind of parallel robot that replaces traditional rigid links with cables. CDPRs have many advantages over traditional parallel robots, such as simple structure, large workspace, low inertia of moving parts, fast-moving speed, high modularity and low cost [1–3]. It is widely used in radio telescopes, [4] tactile interaction, [5] construction tasks, [6] high-speed pick and place manipulators [7] and other fields. Since the 1980s, the CDPR has been a research hotspot in the field of robotics and attracted the attention of many researchers [8,9].

With the continuous innovation and development in modern manufacturing and scientific technologies, robots need to carry out many tasks at the same time and work in more complex environments, which results in higher requirements for the robots' performance. The error of robots can be defined as the deviation between the theoretical position orientation and the actual position orientation, which is a significant problem in the industries that demand high precision on the completion of robots' tasks [10–13]. As for a CDPR, the rigid-flexible coupling in the structural design, manufacturing, assembly process and other factors can lead to its failure in achieving the desired precision. A CDPR is required not only for operations with high accuracy but also applications with greater flexibility. Therefore, it is essential to conduct error analysis for a CDPR.

Some research has been conducted on the error modeling and sensitivity analysis of parallel robots. The basic method for dealing with the error modeling of parallel robots is based on D-H parameter analysis method. Many scholars have proposed the influence coefficient method, the position and orientation error significance analysis and the distance error analysis for the parallel robots. Maurine et al. [14] established the error mapping model of 3-DOF parallel robot Delta 4 by the coordinate transformation method and dealt with sensitivity analysis. A two-stage calibration method for the parallel robot Delta 4 is presented. The results revealed the robustness of the protocol and validated this procedure.

© The Author(s), 2021. Published by Cambridge University Press.

https://doi.org/10.1017/S0263574721001582 Published online by Cambridge University Press

The simulation showed that the random errors should be less than 0.3 mm to have the accuracy about $\pm 0.1^{\circ}$ for the orientation and the offsets errors, and the identification procedure is robust with respect to these variations. This method can allow one to identify the absolute location of the robot base and the offsets on the three first joints. Nevertheless, the problem still existed that the contribution of each error component to the parallel robot Delta 4 cannot be calculated. Wang et al. [15] established the error modeling of Stewart platform of 6-DOF and analyzed the position and orientation accuracy of the robot while considering the errors of spherical hinge and limb length. The method of sensitivity analysis can describe the contribution of each error component to the total position and orientation error of the mechanism, which was useful to understand the character and propagation of errors of 6-DOF Stewart platform.

There are also some studies on error modeling and sensitivity analysis of CDPRs. Reicherts et al. [16] proposed a method for the accurate estimation of the kinematic parameters of a CDPR, where the calibration process was simplified, and the calibration accuracy was improved through sensitivity analysis of the CDPR. The results showed that the parameter influence generally decreases with its interaction level. This characteristic can be explained by the kinematic loops, which is a particular property of the CDPR. The parameter effects and interactions were calculated to carry out the sensitivity analysis, but local sensitivity of the kinematic parameters like the cable length was not presented, and it is important to determine the sensitivity kinematic parameters. Baklouti et al. [17] carried out a sensitivity analysis of geometric and mechanical uncertainties for the CDPR to achieve robust control which is based on elastic geometric models. Considering 62 geometric and mechanical error sources, the effects of external loads on static deflection of the moving platform of the CDPR were analyzed. The proposed model was verified for the purpose of model-based control of the CDPR. This research revealed that the integrating cables hysteresis effect on the error modeling is important to enhance the cables' mechanical behavior, especially when there was no feedback about tension measurement. However, a better error modeling can be used for the calibration and identification of geometrical parameters. There were some limitations on the research of the error local sensitivity and sensitivity coefficient. Aref et al. [18] studied the impact of mechanical assembly tolerances on the closed-loop control performance of a CDPR, where the sensitivity analysis of the precision in the construction and assembly of the system was performed in the closed loop. The results of the research indicated that most of position and orientation errors of the CDPR are originating from the components. The induced errors are caused by mechanical and measurement errors in this research, which leads to the result that the error mapping function of the CDPR is not obvious. Therefore, the uncompensated error sources can be controlled through error analysis, which is helpful for the minimization of error [19]. The sources of error for uncompensated errors can be eliminated or minimized according to the sensitivity of the system response to each error source [20,21]. The approach is helpful to determine the parameters of the mechanism and the dynamic analysis of the system during the design process [22]. The studies of error modeling and sensitivity analysis can be used for the optimization design, error compensation and accuracy synthesis of the CDPR.

In these above-mentioned former works, the robots are either rigid-body robots or robots only driven by cables. Although the influence of pulleys is obviously one of the error sources of cable-driven mechanisms, it is rarely concerned in error analyses of CDPR, as pulleys are simplified to be ideal points in many works [23]. In this paper, the conceptual design of a CDPR driven by the mixed action of the cables and a limb is developed. A method which can be used for the error modeling and sensitivity analysis of this kind of CDPR is provided. By combining the inverse position analysis with the relationship between cables' length and pulleys' radius, the error mapping model of the CDPR is established efficiently. This model can be applicable for the parallel robots with the characteristics of rigid-flexible coupling. Through sensitivity analysis including the error local sensitivity and the error sensitivity coefficients, the influence of each source of error can be presented visually. Except for the ability to graphically depict the error distribution throughout the workspace, it is instrumental in selecting the best regions in the workspace to perform the work.

The overall work of this paper is listed as follows. In Section 2, the conceptual design of the CDPR is carried out and the final mechanical design scheme is determined. The description of the mechanical

https://doi.org/10.1017/S0263574721001582 Published online by Cambridge University Press

Table I. *Degrees of freedom and types of motion of mechanisms.*

Dof type	Number of cables	Dof of moving platform	Motion type
1T	2	1	Linear motion of rigid body
2T	3	2	Plane motion of a point
1R2T	4	3	Plane motion of rigid body
3T	5	4	Linear motion of a point
2R3T	6	5	Spatial motion of line
3R3T	7	6	Spatial motion of rigid body

Table II. *Comparison of the characteristics of schemes.*

Scheme	Number of Dof	Number of cables	Cost	Types of mechanisms
Scheme 1	2	3	Low	Completely restrained mechanism
Scheme 2	2	4	High	Redundantly restrained mechanism

structure and kinematics analysis of the CDPR are introduced in Section 3. The geometric error modeling and analysis of the CDPR based on kinematics are provided in Section 4. The sensitivity analysis based on the error modeling is presented in Section 5. In Section 6, the numerical examples are carried out to verify the validity of the error modeling and sensitivity error sources of the CDPR. The conclusions are given in Section 7.

2. Conceptual design of a CDPR

A CDPR with two rotational degrees of freedom can be designed for fields like wind tunnel testing, [25] patient rehabilitation [26] and wearable equipment [27]. The inertia of the CDPR is reduced due to the use of the light-weight cable instead of the rigid link as the transmission component, and the CDPR has a higher ration of load capacity/weight.

Most of the cable-driven parallel mechanisms connect one side of the cable to the moving platform, and the other side is connected to the motor through a fixed platform. The tension cable has a certain rigidity, so it can be equivalent to the effect of a moving pair in theory [24]. As the flexible cable can only bear tension along its axis direction instead of pressure, n cables cannot realize the complete constraint of n degrees of freedom position. At least $(n + 1)$ cables are needed to realize the complete constraint of position, and the extra one or more cables are used to ensure that all the driving cables in the mechanism are in tension state. As a result, CDPRs can be divided into the following three categories according to the relationship between the degrees of freedom of the platform n and the number of cables m [28]: (i) incompletely restrained mechanisms ($m \leq n$), (ii) completely restrained mechanisms ($m = n + 1$) and (iii) redundantly restrained mechanisms ($m > n + 1$). And the completely restrained cable mechanisms can be divided into the following types, as shown in Table I.

According to the above analysis of the degree of freedom and the type of motion, it can be determined that a CDPR with two degrees of freedom needs three cables to realize its expected motion. As for the redundantly restrained mechanism, there can be four cables, each two cables in the opposite positions drive one degree of freedom. Both the completely restrained mechanism and the redundantly restrained mechanism are useful in some applications, so they are both considered and designed. Comparison of the characteristics of the two schemes are given in Table II. The flow charts of conceptual design schemes of the CDPR are given in Fig. 1.

The above-mentioned conceptual designs shown in Fig. 1 can both achieve the expected motion, but there are differences in working performances. Considering the cost and the complexity of control, [29] the design of Scheme 1 is better than that of Scheme 2. In order to simplify the model and facilitate the calculation, the Scheme 1 is investigated in this paper.

https://doi.org/10.1017/S0263574721001582 Published online by Cambridge University Press

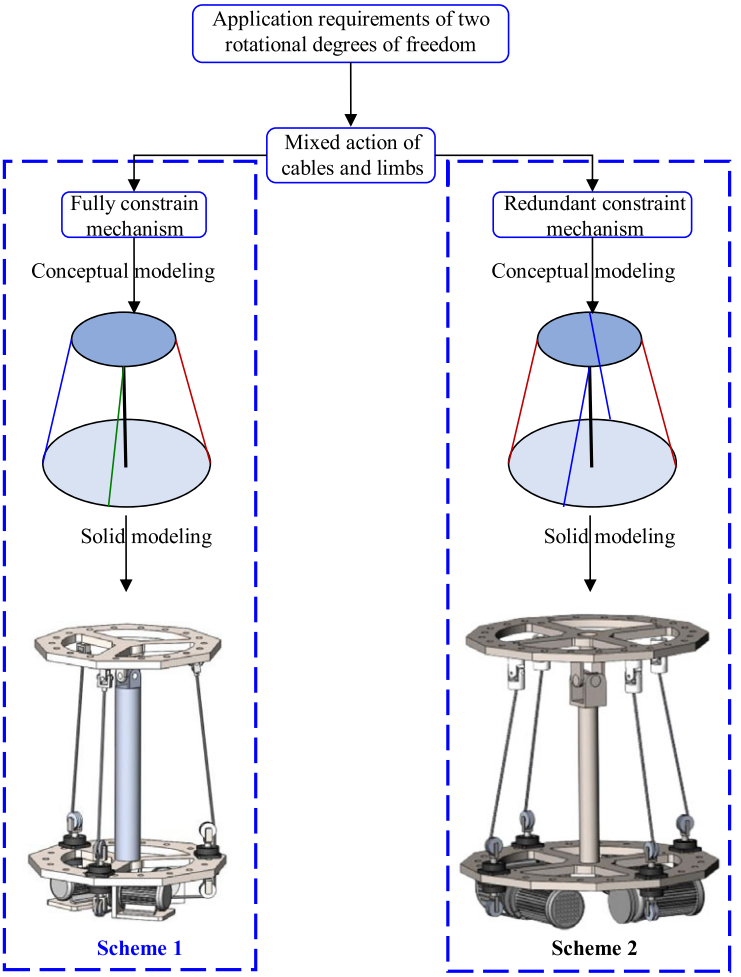


Figure 1. *The flow charts of conceptual design schemes of the CDPR.*

3. Kinematics analysis of the CDPR

3.1 Structure description

A three-dimensional model of a CDPR is shown in Fig. 2(a). This structure consists of a moving platform, a base platform, three external cable-driven chains and a fixed-length limb chain. The three external cable-driven chains are the same as each other. One end of the three cable-driven branching chains is connected with the moving platform through a universal joint. The other end is coiled on the motor through a pulley. Motors are placed under the base platform. The three cable branching chains of the CDPR are distributed outside. Each cable is driven by a motor, and all the cables are axis symmetrically distributed in space. One end of the supporting chain of the fixed-length limb is connected with the moving platform through the universal joint, and the other end is vertically fixed with the center of the base platform through bolts, which are placed at the center of the CDPR. The hinge points of both the moving platform and the base platform are designed to be placed at the vertex of the triangle.

Figure 2(b) shows the structural scheme of the CDPR. Point A_i and B_i ($i = 1,2,3$) represent the center point of the cable-driven branched pulley and the cable-supported universal joint, respectively. On the base platform and moving platform, the distribution is designed to be an equilateral triangle.

https://doi.org/10.1017/S0263574721001582 Published online by Cambridge University Press

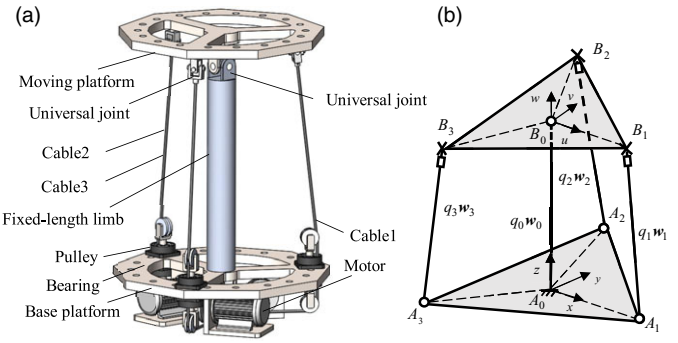


Figure 2. *The CDPR: (a) three-dimensional model of the CDPR and (b) structure diagram of the CDPR.*

The central fixed-length limb connects the base platform and moving platform on the point A_0 and B_0, respectively.

3.2 Kinematic model

As shown in Fig. 2(b), a fixed coordinate system A_0-xyz is established on the center point A_0 of the base platform. The x-axis points in the direction of point A_0 to point A_1, and the vertical base platform of the z-axis points to the moving platform. The y-axis satisfies the right-hand rule. A fixed coordinate system B_0-uvw is established on the center point B_0 of the moving platform, in which the u-axis is pointed in the direction from point B_0 to point B_1, and the w-axis is perpendicular to the plane of the moving platform, and the v-axis satisfies the right-hand rule. To establish the kinematics model of the CDPR and simplify the subsequent calculation, the universal joints of the three cable-driven branches and the universal joints of the fixed-length limb branches are all located on the moving platform, and the pulleys of the three cable-driven branches are all located on the base platform. Therefore, the center point B_0 of the moving platform can be described by position vector r and rotation matrix ${}^{A_0}\boldsymbol{R}_{B_0}$, which is defined as the rotation matrix from the moving platform to the base platform. It can be expressed by three Euler angles, namely rotates angle ϕ_x first around the fixed x-axis and then rotates with the angle ϕ_y around the fixed y-axis and finally rotates with the angle ϕ_z around the fixed z-axis. So ${}^{A_0}\boldsymbol{R}_{B_0}$ can be written as

$$ {}^{A_0}\boldsymbol{R}_{B_0} = \mathrm{Rot}(z, \phi_z)\mathrm{Rot}(y, \phi_y)\mathrm{Rot}(x, \phi_x) \tag{1} $$

where

$$ c\phi_x = \cos\phi_x, s\phi_x = \sin\phi_x \tag{2} $$

As shown in Fig. 3, the coordinate system A_i-$x_iy_iz_i(i = 1,2,3)$ is established at point A_i to describe the cable-driven branching chain. The orientation rotation angle of each cable-driven branched-chain in the base platform coordinate system can be expressed by two Euler angles. It can be regarded as a rotation with the angle β_{ei} about the z-axis resulting in the coordinate system B_i-$x_i'y_i'z_i'$ followed by another angle θ_{ei} about the rotated y_i'-axis. ${}^{A_0}\boldsymbol{R}_i$ is defined as the rotation change matrix from the connected coordinate system to the base platform fixed coordinate system. Therefore, ${}^{A_0}\boldsymbol{R}_i$ can be obtained as

$$ {}^{A_0}\boldsymbol{R}_i = \mathrm{Rot}(z, \beta_{ei})\mathrm{Rot}(y'_i, \theta_{ei}) \tag{3} $$

The unit vectors $\boldsymbol{w}_0$ of the fixed-length limb A_0B_0 and the unit vectors $\boldsymbol{w}_i$ of the cable branched-chain A_iB_i are described as

$$ \boldsymbol{w}_0 = \begin{bmatrix} 0 & 0 & 1 \end{bmatrix}^T \tag{4} $$

$$ \boldsymbol{w}_i = {}^{A_0}\boldsymbol{R}_i[\,0 \quad 0 \quad 1\,]^T = \begin{bmatrix} c\beta_{ei}s\theta_{ei} & s\beta_{ei}s\theta_{ei} & c\theta_{ei} \end{bmatrix}^T \tag{5} $$

Therefore, the position orientation rotation angle of the cable-driven branched-chain, Euler angle θ_{ei} and Euler angle β_{ei} can be calculated as

https://doi.org/10.1017/S0263574721001582 Published online by Cambridge University Press

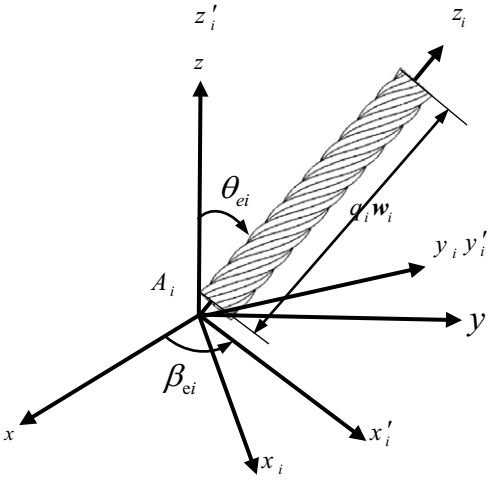


Figure 3. *The local coordinate system of the ith cable.*

$$\begin{cases} c\theta_{ei} = \boldsymbol{w}_{iz} \\ s\theta_{ei} = \sqrt{\boldsymbol{w}_{ix}^2 + \boldsymbol{w}_{iy}^2}, (0 \le \theta_{ei} < \pi) \\ c\beta_{ei} = \boldsymbol{w}_{ix}/s\theta_{ei} \\ s\beta_{ei} = \boldsymbol{w}_{iy}/s\theta_{ei} \\ \text{if}\theta_{ei} = 0, \quad \text{then} \quad \beta_{ei} = 0 \end{cases} \tag{6}$$

3.3 Inverse position analysis

As shown in Fig. 2(b), the position closed-loop constraint equation is described as (7) according to the principle of vector closure in the fixed coordinate system of the base platform.

$$\boldsymbol{a}_i + q_i \boldsymbol{w}_i = \boldsymbol{H} + {}^{A_0}\boldsymbol{R}_{B_0}\,{}^{B_0}\boldsymbol{b}_i, (i = 1, 2, 3) \tag{7}$$

The length of the cables can be obtained as

$$q_i = \sqrt{\left(\boldsymbol{H} - \boldsymbol{a}_i + {}^{A_0}\boldsymbol{R}_{B_0}\,{}^{B_0}\boldsymbol{b}_i\right)^T \left(\boldsymbol{H} - \boldsymbol{a}_i + {}^{A_0}\boldsymbol{R}_{B_0}\,{}^{B_0}\boldsymbol{b}_i\right)} \tag{8}$$

where

$$\boldsymbol{H} = q_0 \boldsymbol{w}_0 = \begin{bmatrix} 0 & 0 & h' \end{bmatrix}^T \tag{9}$$

$$\boldsymbol{a}_0 = \begin{bmatrix} 0 & 0 & 0 \end{bmatrix}^T \tag{10}$$

$$\boldsymbol{a}_i = R\begin{bmatrix} c\alpha_i & s\alpha_i & 0 \end{bmatrix}^T \tag{11}$$

$${}^{B_0}\boldsymbol{b}_0 = \begin{bmatrix} 0 & 0 & 0 \end{bmatrix}^T \tag{12}$$

$${}^{B_0}\boldsymbol{b}_i = r\begin{bmatrix} c\gamma_i & s\gamma_i & 0 \end{bmatrix}^T \tag{13}$$

$$\alpha_i = \begin{bmatrix} \alpha_1 & \alpha_2 & \alpha_3 \end{bmatrix}^T = \begin{bmatrix} 0 & \frac{4\pi}{3} & \frac{2\pi}{3} \end{bmatrix}^T \tag{14}$$

$$\gamma_i = \begin{bmatrix} \gamma_1 & \gamma_2 & \gamma_3 \end{bmatrix}^T = \begin{bmatrix} 0 & \frac{4\pi}{3} & \frac{2\pi}{3} \end{bmatrix}^T \tag{15}$$

https://doi.org/10.1017/S0263574721001582 Published online by Cambridge University Press

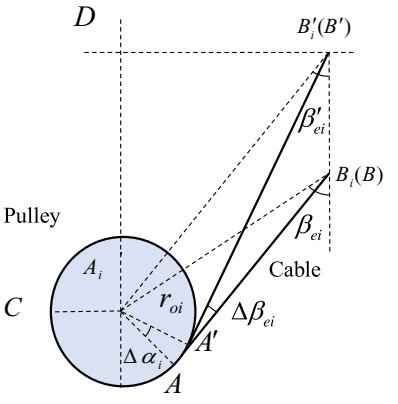


Figure 4. *Systematic structural diagram of a cable passing through the pulley.*

Here, R, r, H, h' , q_i, $\boldsymbol{a}_i$, ${}^{B_0}\boldsymbol{b}_i$, and $\boldsymbol{b}_i$ represent the radius of the base platform, radius of the moving platform, the position vector of point B_0 on the moving platform, the length of the fixed-length limb, the length of cable A_iB_i, the position vector of point A_i expressed in the fixed coordinate system A_0-xyz of the base platform, the position vector of point B_i expressed in the moving coordinate system B_0-uvw, the position vector of point B_i described in the fixed coordinate system A_0-xyz of the base platform, respectively. α_i is the angle between the vector $\boldsymbol{a}_i$ and the x-axis in the fixed coordinate system A_0-xyz, and Γ_i is the angle between the vector ${}^{B_0}\boldsymbol{b}_i$ and the u-axis in the moving coordinate system B_0-uvw.

3.4 Pulley modeling

Earlier analysis of cable-driven robots generally regarded the cable around the pulley as a center point in the theoretical analysis. However, the cable does not pass through one point in the course of the movement when the cable crosses the pulley. The wrap angle of the cable on the pulley also affects the length of the cable, which influences the accuracy of the CDPR [30]. To establish a more accurate error model of the CDPR, it is necessary to take the influence of the pulleys into consideration.

The cable of CDPR passing through the pulley is shown in Fig. 4. A_i is the center of the pulley on the base platform. A is the tangent point between the cable and the pulley. B_i is the hinge point between the cable and the moving platform. Assuming the tangent point between the cable and the pulley is A' after some time, the hinge point between the cable and the moving platform is B_i'. As the change in cable length depends on the radius of the drum connected to the motor, the influence of motor is not considered in this paper. The variation in the actual cable length after movement can be obtained as

$$\Delta l_i = \|A_i'B_i'\| - \|A_iB_i\| = \sqrt{q_i^2 - r_{oi}^2} - \sqrt{q_i'^2 - r_{oi}^2} + \Delta\alpha_i \cdot r_{oi} \tag{16}$$

where Δl_i, $\|A_iB_i'\|$, $\|A_iB_i\|$, r_{oi}, $\Delta\alpha_i$, q_i and q_i' represent the variation of the ith cable length, the length of the ith cable after movement, the initial length of the ith cable, the radius of the ith pulley, the variation of the ith wrap angle, the nominal length of the ith cable before movement and the nominal length of the ith cable after movement, respectively.

According to geometric relations shown in Fig. 4, $\Delta\alpha_i$ can be calculated as

$$\Delta\alpha_i = \left(\beta_{ei} - \arcsin\frac{r_{oi}}{q_i}\right) - \left(\beta_{ei}' - \arcsin\frac{r_{oi}}{q_i'}\right) \tag{17}$$

where β_{ei} and β_{ei}' are calculated in (6).

https://doi.org/10.1017/S0263574721001582 Published online by Cambridge University Press

4. Error analysis

Assume that the processing errors of the cable, moving platform, base platform, middle fixed-length limb and pulleys are dl_i, dr_i, dR_i, dh_i' and dr_{oi}, respectively. The installation point A_i of the cable and the pulley is evenly distributed on the base platform, and the pulley installation angle is β_i, which represents the angle between the vector $\boldsymbol{a}_i$ and the normal vector of the surface of the pulley. The installation point B_i of the cable and the moving platform is evenly distributed on the moving platform, and the cable installation angle is θ_i, which represents the angle between the normal vector along the cable direction and the plane where the moving platform is located. Assembly errors corresponding to the pulley installation angle and the cable installation angle are $d\beta_i$, and $d\theta_i$, respectively. In order to establish the error modeling for the CDPR, (17) can be rewritten as

$$f_i(r_{oi}, \phi_x, \phi_y, \phi_z, \beta_i, \theta_i, h_i', R_i, r_i, l_i) = 0, (i = 1, 2, 3) \tag{18}$$

By differentiating (18) with respect to all the variables

$$\begin{aligned} &\frac{\partial f_i}{\partial r_{oi}} dr_{oi} + \frac{\partial f_i}{\partial \phi_x} d\phi_x + \frac{\partial f_i}{\partial \phi_y} d\phi_y + \frac{\partial f_i}{\partial \phi_z} d\phi_z + \frac{\partial f_i}{\partial \beta_i} d\beta_i \\ &+ \frac{\partial f_i}{\partial \theta_i} d\theta_i + \frac{\partial f_i}{\partial h'_i} dh'_i + \frac{\partial f_i}{\partial R_i} dR_i + \frac{\partial f_i}{\partial r_i} dr_i + \frac{\partial f_i}{\partial l_i} dl_i = 0 \end{aligned} \tag{19}$$

The matrix form of (19) is described as

$$\boldsymbol{Q}\boldsymbol{\varepsilon} = \boldsymbol{U} \tag{20}$$

where

$$\boldsymbol{Q} = \begin{bmatrix} Q_{i\phi_x} & Q_{i\phi_y} & Q_{i\phi_z} \end{bmatrix} \tag{21}$$

$$\boldsymbol{Q}_{i\phi_x} = \begin{bmatrix} Q_{1\phi_x} & Q_{2\phi_x} & Q_{3\phi_x} \end{bmatrix}^T \tag{22}$$

$$\boldsymbol{Q}_{i\phi_y} = \begin{bmatrix} Q_{1\phi_y} & Q_{2\phi_y} & Q_{3\phi_y} \end{bmatrix}^T \tag{23}$$

$$\boldsymbol{Q}_{i\phi_z} = \begin{bmatrix} Q_{1\phi_z} & Q_{2\phi_z} & Q_{3\phi_z} \end{bmatrix}^T \tag{24}$$

$$Q_{i\phi_x} = \frac{\partial f_i}{\partial \phi_x}, Q_{i\phi_y} = \frac{\partial f_i}{\partial \phi_y}, Q_{i\phi_z} = \frac{\partial f_i}{\partial \phi_z} \tag{25}$$

$$\boldsymbol{\varepsilon} = \begin{bmatrix} d\phi_x & d\phi_y & d\phi_z \end{bmatrix}^T \tag{26}$$

$$\boldsymbol{U} = \begin{bmatrix} U_1 & U_2 & U_3 \end{bmatrix}^T \tag{27}$$

$$U_i = \boldsymbol{C}_i \boldsymbol{\delta p}_i \tag{28}$$

$$\boldsymbol{C}_i = \begin{bmatrix} -\frac{\partial f_i}{\partial r_{oi}} & -\frac{\partial f_i}{\partial \beta_i} & -\frac{\partial f_i}{\partial \theta_i} & -\frac{\partial f_i}{\partial h'_i} & -\frac{\partial f_i}{\partial R_i} & -\frac{\partial f_i}{\partial r_i} & -\frac{\partial f_i}{\partial l_i} \end{bmatrix} \tag{29}$$

$$\boldsymbol{\delta p}_i = \begin{bmatrix} dr_{oi} d\beta_i & d\theta_i & dh'_i & dR_i & dr_i & dl_i \end{bmatrix}^T \tag{30}$$

Here, ϵ represents the orientation error of the center point of the CDPR's moving platform. $\Delta \boldsymbol{p}_i$ represents the collection of error sources including the size error, assembly error and driving error of the moving platform, base platform and middle fixed-length limb. $\boldsymbol{C}_i$ represents the orientation error coefficient matrix related to the mechanical structure of the CDPR.

https://doi.org/10.1017/S0263574721001582 Published online by Cambridge University Press

According to (23), the error mapping function of the CDPR can be transferred as

$$\boldsymbol{\varepsilon} = \boldsymbol{MC}_i \boldsymbol{\delta p}_i \tag{31}$$

where $\boldsymbol{M}$ is the error transfer matrix of the CDPR, which represents the path expression of the error from the design variable (r_{o1},r_{o2},r_{o3},R_1,R_2,R_3,r_1,r_2,r_3,h'_1,h'_2,h'_3,β_1,β_2,β_3,θ_1,θ_2,θ_3) and the driving cable space (l_1,l_2,l_3) to the orientation space (ϕ_x,ϕ_y,ϕ_z) of the moving platform.

5. Sensitivity analysis

According to the previous error analysis and modeling, there are 21 static sources of error in the CDPR. To facilitate further analysis and calculation, a sensitivity model is established to analyze the influence of each error on the position orientation accuracy of the moving platform of the parallel mechanism [31–33]. When the number of error components in the source of a mechanism error is large enough, and the position orientation errors of the end effector and the error components are independent random variables, the errors obey a normal distribution [34]. Because the action mechanisms between errors are complicated, this paper considers the case that the error components are independent for each other. Assuming that each error obeys the standard normal distribution, the variance of ϵ can be calculated as

$$D(\boldsymbol{\varepsilon}) = E(\boldsymbol{\varepsilon}^2) = \sum_{j=1}^{21} \left(\sum_{i=1}^{3} \lambda_{ij}^2 \right) E(\boldsymbol{\delta} p_{ij}^2) \tag{32}$$

where

$$\boldsymbol{\lambda}_i = \boldsymbol{MC}_i, (i = 1, 2, 3) \tag{33}$$

Here, Λ_{ij} represents the ith row and the jth column element in Λ_i. Δp_{ij} represents the jth element in $\boldsymbol{\delta p}_i$.

Because the three cable branches of the CDPR are evenly distributed in space, the mean value of Δp_{ij} can be obtained as

$$E(\boldsymbol{\delta} p_{ij}^2) = E(\boldsymbol{\delta} p_{1j}^2) = E(\boldsymbol{\delta} p_{2j}^2) = E(\boldsymbol{\delta} p_{3j}^2) \tag{34}$$

Combining (33) and (34) into one expression, the standard deviation of ϵ can be obtained as

$$\sigma(\boldsymbol{\varepsilon}) = \sqrt{\sum_{j=1}^{21} \left(\sum_{i=1}^{3} \lambda_{ij}^2 \right) E(\boldsymbol{\delta} p_{ij}^2)} = \sqrt{\sum_{j=1}^{21} S_j^2 D(\boldsymbol{\delta} p_{ij})} \tag{35}$$

where

$$S_j = \sqrt{\sum_{i=1}^{3} \lambda_{ij}^2}, (j = 1, 2, \cdots 21) \tag{36}$$

Here, $\sigma(\varepsilon)$ represents the standard deviation of orientation error. S_j represents the local sensitivity of orientation error ϵ at the center point of the moving platform of the CDPR to the 21 error sources.

It is shown that λ_{ij} varies with the orientation of the moving platform of the CDPR and the sensitivity matrix [35] cannot be calculated directly due to the nonlinearity of the elastic geometry model of the cable in (32). For the traditional variance-based global sensitivity analysis, the total influence of an individual variable commonly involves the interactions with other variables [36]. Therefore, taking its global mean value in the overall workspace as a global average sensitivity of the CDPR and setting it as $\bar{S}_j$, it can be expressed as

$$\bar{S}_j = \frac{\int_V S_j dV}{V} \tag{37}$$

https://doi.org/10.1017/S0263574721001582 Published online by Cambridge University Press

Table III. *Structure parameters of the CDPR.*

Parameters	r **(mm)**	R **(mm)**	r_{oi} **(mm)**	h' **(mm)**	β_i **(rad)**	θ_i **(rad)**	$\psi_{\max}$ **(rad)**
value	120	160	15	190	Π/3	Π/3	Π/6

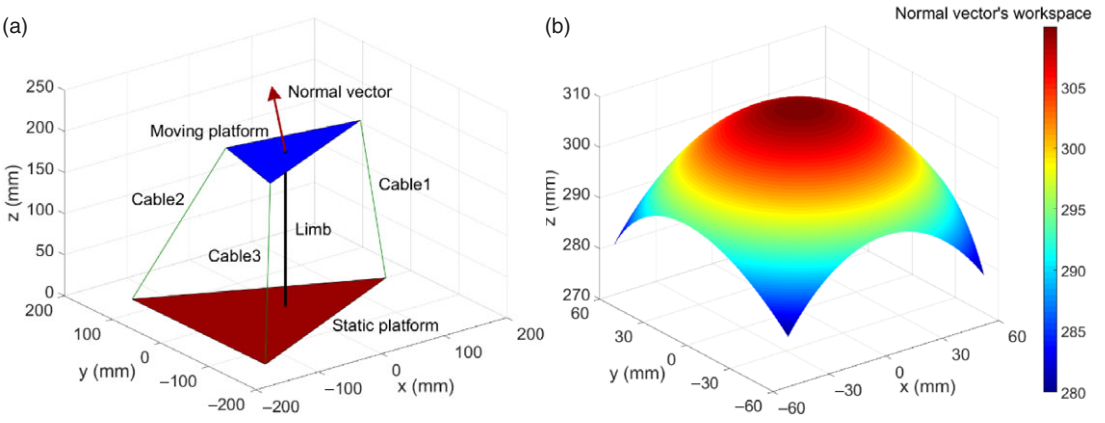


Figure 5. *CDPR: (a) simplified diagram and (b) normal vector reachable workspace of moving platform.*

where V represents the design space of the CDPR. To identify, analyze and compare the sources of sensitive error, the global average sensitivity of the CDPR is treated by standardized dimensionless processing [37]. The error sensitivity coefficients corresponding to each error source are obtained as

$$K_j = \sqrt{\frac{1}{n-1}\sum_{j=1}^{n}\left(S_j^* - \frac{1}{n}\sum_{j=1}^{n}S_j^*\right)^2}, (n=21) \tag{38}$$

where

$$S_j^* = \frac{\bar{S}_j - \frac{1}{n}\sum_{j=1}^{n}\bar{S}_j}{\sqrt{\frac{1}{n-1}\sum_{j=1}^{n}\left(\bar{S}_j - \frac{1}{n}\sum_{j=1}^{n}\bar{S}_j\right)^2}} \tag{39}$$

Here, K_j represents the error sensitivity coefficients, S_j^* represents the standardization of data between the mean and standard deviation of error local sensitivity, so that $\bar{S}_j$ of different units or orders of magnitude can be compared and weighed easily. It satisfies $\sum_{j=1}^{21} K_j = 1$. Therefore, (38) describes the error sensitivity model of the CDPR in a statistical sense.

6. Example and results

The structure parameters of the CDPR are shown in Table III. As shown in Fig. 5(a), the position of the center point of the moving platform remains unchanged, so the workspace of the parallel mechanism cannot be described by the position of the center point of the moving platform. During the movement of the CDPR, the position orientation of the center point of the moving platform can be determined by the endpoint of the unit normal vector of the center point. Therefore, for the center point of the moving platform, the unit normal vector's endpoints are adopted to represent the motion space of the CDPR.

https://doi.org/10.1017/S0263574721001582 Published online by Cambridge University Press

Table IV. *Variance of the error sources for the CDPR.*

No.	$D(\varepsilon)$ (mm/m)^2	$i=1$	$i=2$	$i=3$
1	Δr_{oi}	0.000300	0.000300	0.000300
2	$\Delta \beta_i$	0.000001	0.000001	0.000001
3	$\Delta \theta_i$	0.000001	0.000001	0.000001
4	$\Delta h'_i$	0.000140	0.000140	0.000140
5	ΔR_i	0.000140	0.000140	0.000140
6	Δr_i	0.000120	0.000120	0.000120
7	Δl_i	0.000100	0.000100	0.000100

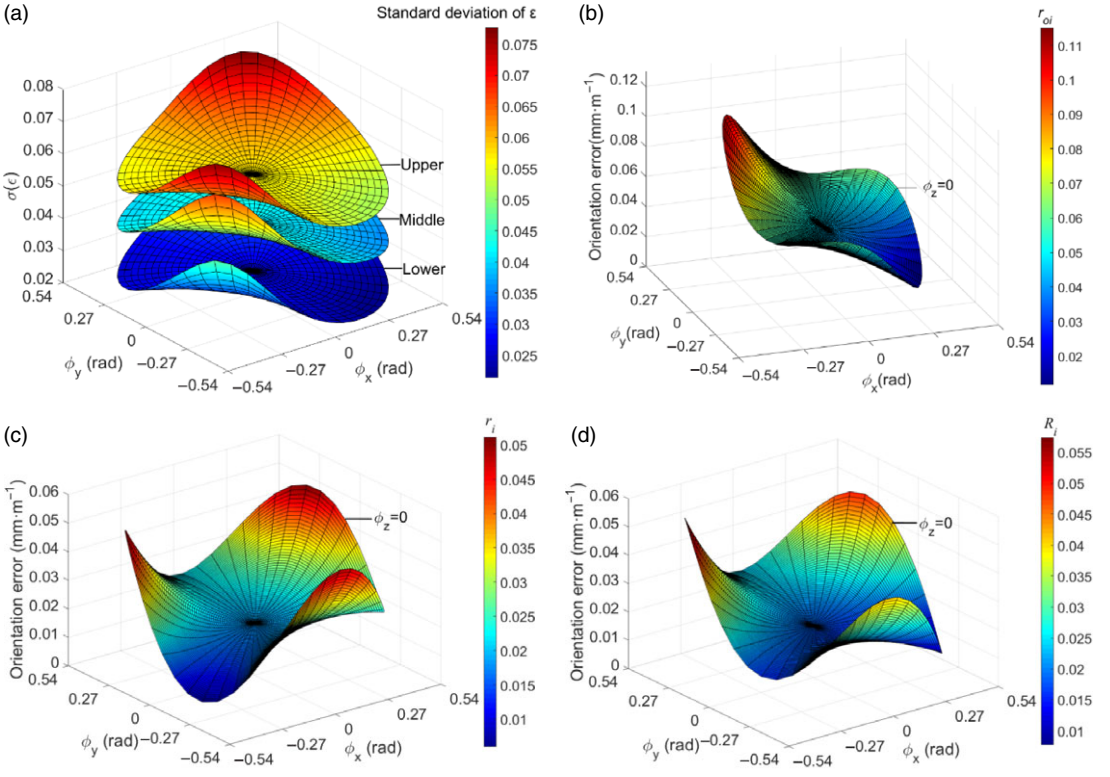


Figure 6. *Distribution of $\Sigma(\epsilon)$ and the orientation errors of the moving platform: (a) distribution of $\sigma(\epsilon)$ in different spatial levels, (b) orientation error only considering r_{oi}, (c) orientation error only considering r_i and (d) orientation error only considering R_i.*

It is assumed that the rotation angle of the universal joint in the CDPR is ψ and its maximum rotation angle is $\psi_{\max}$. The normal unit vector of the center point of the moving platform is expressed as $\boldsymbol{n}_p$ in the moving coordinate system B_0-*uvw*, so the constraint conditions of the rotation angle of the universal joint can be expressed as

$$\psi = \arccos \frac{\boldsymbol{H}\left({}^{A_0}\boldsymbol{R}_{B_0}\boldsymbol{n}_p\right)}{\|\boldsymbol{H}\|} \le \psi_{\max} \tag{40}$$

where

$$\boldsymbol{n}_p = r\begin{bmatrix}0 & 0 & 1\end{bmatrix}^T \tag{41}$$

The normal vector workspace of the CDPR's moving platform is shown in Fig. 5(b). The design space of the CDPR is taken as the area which is enclosed by $z_0 = 290$ mm, $z_f = 300$ mm and the normal

https://doi.org/10.1017/S0263574721001582 Published online by Cambridge University Press

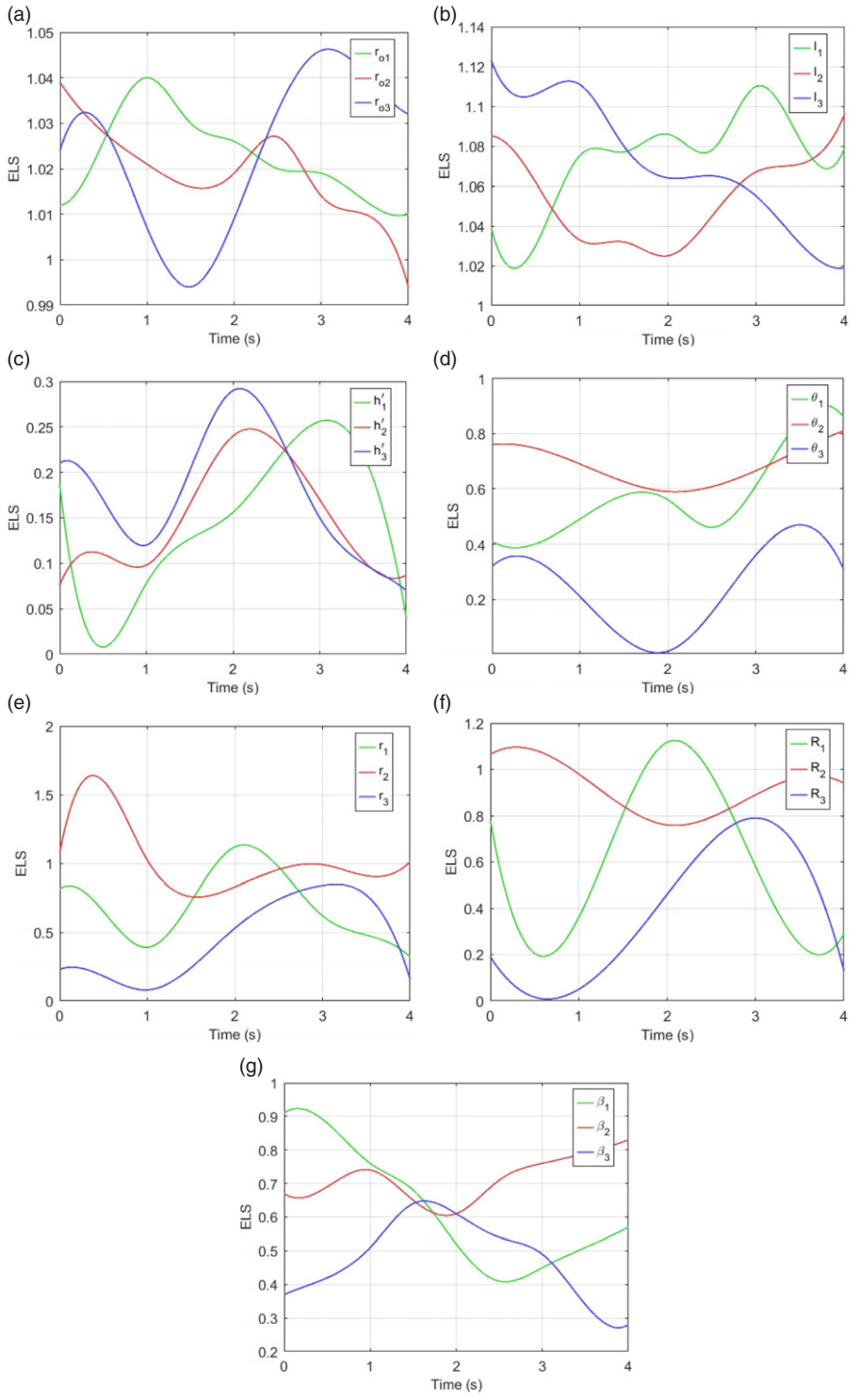


Figure 7. *Error local sensitivity of various parameter error sources: (a) ELS of r_{oi}, (b) ELS of l_i, (c) ELS of h'_i, (d) ELS of θ_i, (e) ELS of r_i, (f) ELS R_i and (g) ELS of β_i.*

https://doi.org/10.1017/S0263574721001582 Published online by Cambridge University Press

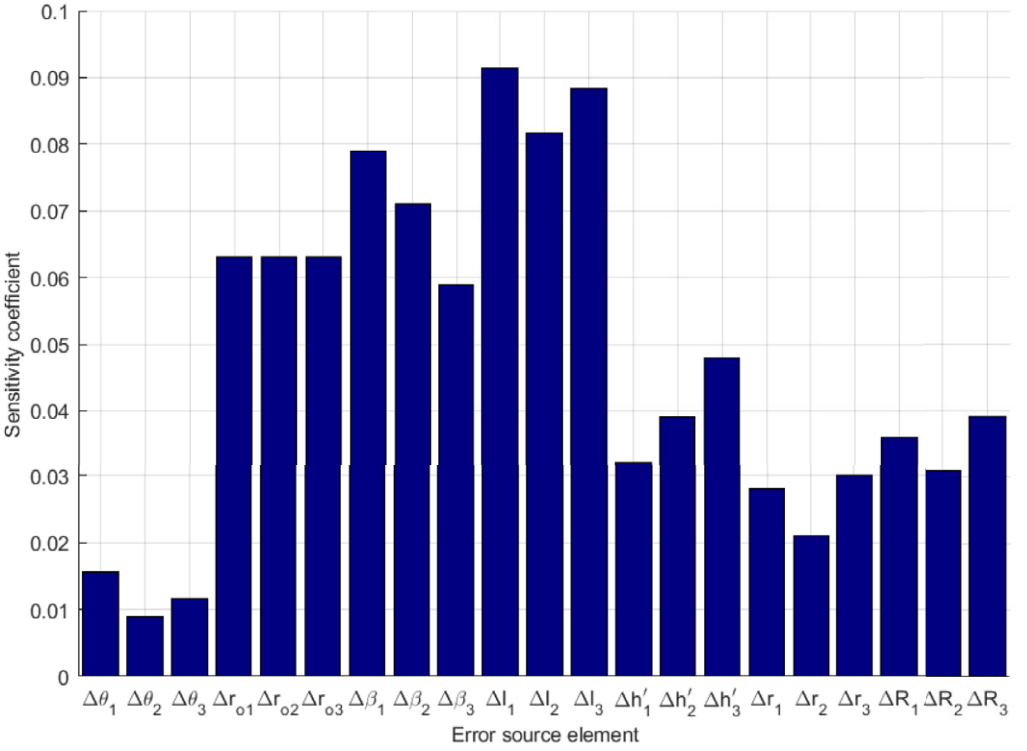


Figure 8. *Histogram of the error sensitivity coefficients of various error sources.*

vector workspace of the moving platform. The length of the three cables is $l_i = 200$ mm. The motion law of servo motor is as follows: $\theta_i = \Omega t\text{-}\cos\beta_i$, $\Omega = 0.5$ rad/s. The trajectory of the CDPR is in (42), where t and T are the run time and motion period:

$$\begin{cases} \phi_x = 0.35[35(t/T)^4 - 84(t/T)^5 + 70(t/T)^6 - 20(t/T)^7] \\ \phi_y = 0.35[35(t/T)^4 - 84(t/T)^5 + 70(t/T)^6 - 20(t/T)^7] \end{cases} \tag{42}$$

The rand function in the MATLAB software is employed to generate randomly the variance of the 21 error sources of the CDPR in a statistical sense, which obeys the normal distribution and its mean value is zero, as shown in Table IV.

When calculating the standard deviation of the orientation error of the moving platform of the CDPR in the design space, the space is divided into upper, middle and lower layers. The angle ϕ_z of each layer are $\phi_{z1} = 0.54$ rad, $\phi_{z2} = 0.27$ rad and $\phi_{z3} = 0$ rad, respectively. The geometric parameter error with zero mean value is selected randomly. The standard deviation of linear error is 0.01 mm, and the standard deviation of angle error is 0.02 mm/m. For the geometric errors of the moving platform, base platform and pulleys, the orientation error distribution for the moving platform of the CDPR is calculated by Monte Carlo method in the whole workspace and $\phi_{z3} = 0$ rad under the premise of controlling the variables. Because the local sensitivity of the error is only the sensitivity of the CDPR in the local design space, the running time of the CDPR is set as 4 s. The standard deviation of the orientation error of the CDPR's moving platform with different parameters and spatial levels, the error local sensitivity curve of each error source and the sensitivity coefficients bar chart are shown in Figs. 6–8, respectively.

As shown in Fig. 6(a), the error standard deviation of the CDPR's moving platform increases with the angle ϕ_z, and the error standard deviation in the upper space is more significant than that in the middle and lower spaces. Compared with Fig. 6(c) and (d), the variation trend of the standard deviation

https://doi.org/10.1017/S0263574721001582 Published online by Cambridge University Press

Table V. *Error sensitivity coefficients of various error sources.*

No.	K_j	$i = 1$	$i = 2$	$i = 3$
1	$\Delta\theta_i$	0.0156	0.0090	0.0117
2	Δr_{oi}	0.0630	0.0630	0.0630
3	$\Delta\beta_i$	0.0790	0.0710	0.0590
4	Δl_i	0.0914	0.0816	0.0884
5	$\Delta h'_i$	0.0323	0.0390	0.0480
6	Δr_i	0.0280	0.0210	0.0300
7	ΔR_i	0.0360	0.0310	0.0390

distribution curve of orientation errors caused by the geometric errors of the moving platform and base platform are the same in the whole working space ($\phi_{z3} = 0$).

As shown in Figs. 7 and 8, the local sensitivity of error sources θ_i, r_{oi}, R_i and β_i are more evident than that of other error sources. The local sensitivity of length errors for the three cables is greater than one. The standard value of the sensitivity coefficient comparison is set as ζ. Since the error sensitivity coefficients of each error source range from 0 and 0.1, $\zeta = 0.05$ is set as a criterion to judge whether each source of error is a sensitive error or not [37].

From the error sensitivity coefficients of Fig. 8 and Table V, it can be seen that the effects of the geometric errors of the pulleys, installation errors of the pulleys and geometric errors of the cable length are relatively larger among the 21 error sources. The sources of sensitivity error in the CDPR can be identified by the standard value of sensitivity coefficient comparison ζ, and they are Δr_{o1}, Δr_{o2}, Δr_{o3}, $\Delta\beta_1$, $\Delta\beta_2$, $\Delta\beta_3$, Δl_1, Δl_2 and Δl_3. From Fig. 6(b), it can be seen that the radius of the pulley has a significant influence on the orientation error of the moving platform.

7. Conclusions

This paper presents the conceptual design of a CDPR with rigid-flexible coupling and guiding pulleys and then deals with its error analysis. The kinematics analysis and error modeling of the CDPR considering the influence of pulleys is formulated. The contribution of each error component to the total orientation error of the CDPR is described by sensitivity analysis. The error analysis of the CDPR including the error's local sensitivity analysis and identification of sources of sensitivity error is presented.

The geometric errors and installation errors affecting the orientation errors of the CDPR's moving platform were refined into 21 sources of error. The geometric errors of the pulleys have a significant influence on the orientation error of the CDPR's moving platform through error analysis, which has guiding significance for the conceptual design. The sensitivity coefficients of pulleys' geometric errors and geometric errors in the cable length are relatively larger among these error sources. Therefore, the importance of manufacturing tolerances for the pulleys is proven. The cable length errors and pulleys' geometric errors should be given higher priority in the design and processing, which provides a guidance for the mechanism optimization and prototype development of a CDPR.

The provided method for the error modeling and sensitivity analysis in this paper can be applied to the CDPR and the parallel mechanisms with rigid-flexible coupling. Based on this method, further researches about precise control of CDPRs can be developed.

Acknowledgements. The authors would like to thank the anonymous reviewers for their very useful comments.

Financial Support. The research is jointly supported by the National Natural Science Foundation of China (Grant No. 51375288), the Science and Technology Program of Guangdong Province (Grant No. 2020ST004), and the Special Project for Science and Technology Innovation Team of Foshan City (Grant No. 2018IT100052).

https://doi.org/10.1017/S0263574721001582 Published online by Cambridge University Press

Conflict of Interest. The authors declare that they have no known competing financial interests or personal relationships that could have appeared to influence the work reported in this paper.

References

[1] P. Bosscher and I. Ebert-Uphoff, "Wrench-based Analysis of Cable-Driven Robots," *Proceedings of 2004 IEEE International Conference on Robotics and Automation (ICRA)* (2004) pp. 4950–4955.

[2] R. Verhoeven and M. Hiller, "Estimating the controllable workspace of tendon-based Stewart platforms," *Advances in Robot Kinematics* (Springer, Dordrecht, 2000) pp. 277–284.

[3] G. Abbasnejad and M. Carricato, "Real solutions of the direct geometrico-static problem of under-constrained cable-driven parallel robots with 3 cables: A numerical investigation," *Meccanica* **47**(7), 1761–1773 (2012).

[4] R. Yao, X. Q. Tang, T. M. Li and G. X. Ren, "Analysis and design of 3T cable-driven parallel manipulator for the feedback's orientation of the large radio telescope," *Chin. J. Mech. Eng-En.* **43**(11), 105–109 (2007).

[5] L. Dominjon, J. Perret and A. Lécuyer, "Novel devices and interaction techniques for human-scale haptics," *Visual. Comput.* **23**(4), 257–266 (2007).

[6] I. B. Hamida, M. A. Laribi, A. Mlika, L. Romdhane, S. Zeghloul, G. Carbone. "Multi-objective optimal design of a cable driven parallel robot for rehabilitation tasks," *Mech. Mach. Theory* online(156):104141 (2021).

[7] A. Gonzalez-Rodriguez, F. J. Castillo-Garcia, E. Ottaviano, P. Rea and A. G. Gonzalez-Rodriguez, "On the effects of the design of cable-driven robots on kinematics and dynamics models accuracy," *Mechatronics* **43**, 18–27 (2017).

[8] J. Albus, R. Bostelman and N. Dagalakis, "The NIST robocrane," *J. Rob. Syst.* **10**(5), 709–724 (1993).

[9] C. Gosselin and M. Grenier, "On the determination of the force distribution inoverconstrained cable-driven parallel mechanisms," *Meccanica* **46**(1), 3–15 (2011).

[10] R. B. He, Y. J. Zhao and S. N. Yang, "Kinematic-parameter identification for serial-robot calibration based on POE formula," *IEEE Trans. Rob*. **26**(3), 411–423 (2010).

[11] H. L. Shi, H. J. Su, N. Dagalakis and J. A. Kramar, "Kinematic modeling and calibration of a flexure based hexapod nanopositioner," *Precis. Eng.* **37**(1), 117–128 (2013).

[12] Y. B. Wang, P. Pessi, H. P. Wu and H. Handroos, "Accuracy analysis of hybrid parallel robot for the assembling of ITER," *Fusion. Eng. Des*. **84**(7-11), 1964–1968 (2009).

[13] J. Santolaria, A. Juan-José, Y. José-Antonio and J. Pastor, "Kinematic parameter estimation technique for calibration and repeatability improvement of articulated arm coordinate measuring machines," *Precis. Eng.* **32**(4), 251–268 (2008).

[14] P. Maurine and E. Dombre, "A Calibration Procedure for the Parallel Robot Delta 4," *Proceedings of 1996 IEEE International Conference on Robotics and Automation (ICRA)* (1996) pp. 975–979.

[15] S. M. Wang and K. F. Ehman, "Errors model and accuracy analysis of a six-DOF stewart platform," *J. Mnuf. Sci. E-T. ASME.* **124**(2), 519–530 (1995).

[16] S. Reicherts, S. Blume, C. Reichert, D. Schramm, "Sensitivity analysis of the design parameters for the calibration of cable-driven parallel robots," *Pamm.* **16**(1), 859–860 (2016).

[17] S. Baklouti, S. Caro and E. Courteille, "Sensitivity analysis of the elasto-geometrical model of cable-driven parallel robots," *Cable-Driven Parallel Robots. Mechanisms and Machine Science* (Springer, Cham, 2018) pp. 37–49.

[18] M. M. Aref, P. Gholami and H. D. Taghirad, "Dynamic and Sensitivity Analysis of KNTU CDRPM: A Cable Driven Redundant Parallel Manipulator," *Proceedings of 2008 IEEE/ASME International Conference on Mechtronic and Embedded Systems and Applications (MESA)* (2008) pp. 528–533.

[19] Z. C. Shi and S. H. Liu, *Institutional accuracy*, (CHEP, Beijing, 1995).

[20] H. Liu, T. Huang and D. G. Chetwynd, "A general approach for geometric error modeling of lower mobility parallel manipulators," *J. Mech. Robot.* **3**(2), 021013 (2011).

[21] T. Huang, Y. Li, G. B. Tang, S. W. Li, X. Y. Zhao, D. J. Whitehouse, D. G. Chetewyn and X. P. Liu, "Error modeling, sensitivity analysis and assembly process of a class of 3-DOF parallel kinematic machines with parallelogram struts," *Sci. China. Ser. E.* **45**(5), 467–476 (2002).

[22] Z. Zi, "Sensitivity analysis approaches applied to systems biology models," *IET. Syst. Biol.* **5**(6), 336–346 (2011).

[23] A. Pott, "Influence of Pulley Kinematics on Cable-Driven Parallel Robots," In: *Latest Advances in Robot Kinematics* (2012) pp. 197–204.

[24] G. H. Cui, Y. W. Zhang, Y. S. Zhang and W. J. Hao, "Configuration design and analysis of a new 3-SPS/S spatial rotation parallel manipulator," *J. Jilin. U Technol. Ed.* **39**(S1), 200–205 (2009).

[25] X. Liu, Y. Y. Qiu and Y. Sheng, "Stiffness enhancement and motion control of a 6-DOF wire-driven parallel manipulator with redundant actuations for wind tunnels," *Acta. Aeronau. Astronaut. Sin.* **30**(006), 1156–1164 (2009).

[26] G. Rosati, P. Gallina and S. Masiero, "Design, implementation and clinical tests of a wire-based robot for neurorehabilitation," *IEEE Trans. Neur. Syst. Reh*. **15**(4), 560–569 (2007).

[27] M. Ying and S. K. Agrawal, "Wearable Cable-Driven Upper Arm Exoskeleton-Motion with Transmitted Joint Force and Moment Minimization," *Proceedings of 2010 IEEE International Conference on Robotics and Automation (ICRA)* (2010) pp. 4334–4339.

[28] R. Verhoeven, Analysis of the Workspace of Tendon-Based Stewart Platforms *Ph.D. Thesis* (University of Duisburg-Essen, 2004).

https://doi.org/10.1017/S0263574721001582 Published online by Cambridge University Press

[29] Y. J. Zhao, F. Gao, X. J. Dong and X. C. Zhao, "Elastodynamic characteristics comparison of the 8-PSS redundant parallel manipulator and its non-redundant counterpart—the 6-PSS parallel manipulator," *Mech. Mach. Theory* **45**(2), 291–303 (2010).
[30] P. Gallina and G. Rosati, "Manipulability of a planar wire driven haptic device," *Mech. Mach. Theory.* **37**(2), 215–228 (2002).
[31] Y. Chen, F. Xie, X. Liu and Y. H. Zhou, "Error modeling and sensitivity analysis of a parallel robot with SCARA (Selective Compliance Assembly Robot Arm) motions," *Chin. J. Mech. Eng-En.* **27**(4), 693–702 (2014).
[32] Z. Y. Hong, J. P. Mei, X. M. Zhao and T. Huang, "Error modeling and sensitivity analysis of reconfigurable hybrid robot module Trivariant," *Chin. J. Mech. Eng-En.* **42**(12), 65–69 (2006).
[33] K. C. Fan, H. Wang, J. W. Zhao and T. H. Chang, "Sensitivity analysis of the 3-PRS parallel kinematic spindle platform of a serial-parallel machine tool," *Int. J. Mach. Tool. Manu.* **43**(15), 1561–1569 (2003).
[34] P. Miermeister, W. Kraus, T. Lan and A. Pott, "An elastic cable model for cable-driven parallel robots including hysteresis effects," *Cable-Driven Parallel Robots. Mechanisms and Machine Science* (Springer, Cham, 2015) pp. 17–28.
[35] B. Zi, H. Ding, X. Wu and A. Kecskeméthy, "Error modeling and sensitivity analysis of a hybrid-driven based cable parallel manipulator," *Precis. Eng.* **38**(1), 197–211(2014).
[36] K. Cheng, Z. Z. Lu and K. C. Zhang, "Multivariate output global sensitivity analysis using multi-output support vector regression," *Struct. Multidiscip. O.* **59**(6), 2177–2187 (2019).
[37] B. Zi, *Mechanics analysis and tracking control technology of hybrid-driven based cable parallel robots*, (CSP, Beijing, 2013).

Cite this article: J. Li, Y. Zhao, Q. Tang, W. Sun, F. Yuan and X. Lu (2022). "Conceptual design and error analysis of a cable-driven parallel robot", Robotica **40**, 2152–2167. https://doi.org/10.1017/S0263574721001582

https://doi.org/10.1017/S0263574721001582 Published online by Cambridge University Press